26th ABCM International Congress of Mechanical Engineering
November 22-26, 2021. Florianópolis, SC, Brazil

COB-2021-0047
Modeling and Analysis of a Pitot Tube Pneumatic Installation for Airspeed Using Bond-Graphs

Vinícius Leite de Morais Véras
EMBRAER S.A. - São José dos Campos, SP - Brazil
vinicius.veras@embraer.com.br / viniciuslmveras@gmail.com

Luiz Carlos Sandoval Góes
Instituto Tecnológico de Aeronáutica (ITA) - São José dos Campos, SP - Brazil
goes@ita.br

Abstract. *Aircraft tests require measurements of several parameters, such as airspeed. Airspeed sensors require calibration tests using reference sensors installed in a prototype as a test instrumentation. These reference airspeed sensors are installed using a pipeline, which is subject to pressure (pneumatic) lag. A bond-graph model is proposed herein to represent pneumatic effects such as fluids resistance, capacitance and inductance. The model is implemented on 20-sim software. Time response of the pressure on the end of the line is obtained for a simulated acceleration of the aircraft. The effect of the pressure lag on measured airspeed is then computed for different conditions such as altitude, atmospheric temperature, pipeline length and internal diameter. Effects of those parameters on measured airspeed are then evaluated. Finally, a short rationale on certification requirements is used to substantiate a chart correlating the maximum line length for a specific internal diameter, which is then proposed to be used as a guideline for air data pneumatic installations.*

Keywords: *Pitot tube, Airspeed, Lag, Flight Test, Bond Graph.*

1. INTRODUCTION

A typical airspeed instrumentation is composed by a total pressure Pitot probe installed on aircraft nose. This probe is connected to an electronic transducer by a pipeline (Fig. 1) that goes all the way from aircraft nose to the electronic racks installed inside a test prototype cabin. Pneumatic effects such as pressure loss, compressibility and inertia are considered. As the system is installed inside an aircraft prototype subject to significant accelerations (non-inertial reference), the effects of such acceleration in a magnitude compatible with typical takeoff procedure may be significant on the measured pressures.

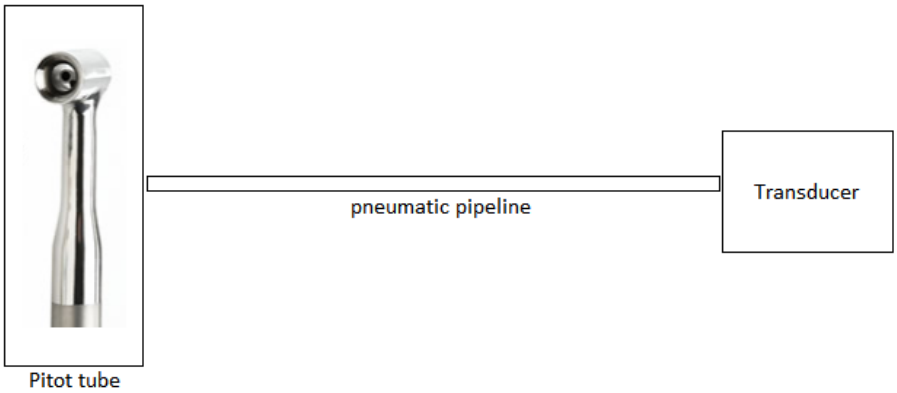

Figure 1. Simulation results without inertia forces effect

As the installation described above may be subject to some errors due to dynamic characteristics such as stabilization time, certification agencies (FAA/EASA/ANAC) evaluate airspeed indication errors. The indication error due to lag is addressed by certification requirement CFR 14 §25.1323(g) and some acceptance criteria are specified by FAA (2018) on its flight test guide for certification of transport category airplanes (AC 25-7D, sec. 33.3.1.1.7).

For simplicity, the scope of this work will be limited to the total pressure sensing. Thus, no error will be assumed for static pressure.

System modeling tools are widely available on the industry. Table 1 presents a summary of some available tools regarding the modeling techniques currently implemented in each one.

A brief analysis performed by the authors identified that a modeling based on Bond-Graphs would be suitable for the purposes of this work due to its flexibility and simplicity, as can be observed in following sections.

Table 1. Some modeling tools and its correspondent modeling techniques

	Modeling Technique		
Tool	Signal	Iconic (Linear Graph)	Bond-Graph
Matlab Simulink ™	X		
Matlab Simscape ™	X	X	
AMEsim ™	X	X	
Scilab	X	X	
20-Sim ©	X	X	X

2. SYSTEM MODELING

A system modeling can be performed using basically two approaches: (i) across-through variables and (ii) effort-flow variables. We adopted the effort and flow variables as this is a common approach in bond-graphs literature, i.e. de Silva (2018). Table 2 shows the variables equivalence used in this work.

Table 2. Analogy for pneumatic systems in terms of effort and flow variables

Variable	**Pneumatic**
Flow (f)	Q (volumetric flow)
Effort (e)	P (pressure)

Prsic *et al.* (2013) propose a BG model for hydraulic long transmission lines using cascaded network of π segments. Grava *et al.* (2015) present a similar model using BG for an electrical transmission line.

2.1 Pneumatic Resistance (R_f)

The pneumatic resistance is defined in terms of effort ($e \equiv P$) and flow ($f \equiv Q$) variables as in Eq. (1).

$$R_f = \frac{e}{f} \equiv \frac{P}{Q} \tag{1}$$

Only a small airflow (Q) is expected to occur through the total pressure Pitot end, and such airflow reduces along the pipeline as its transducer end is closed. Thus, the flow regime is assumed laminar and the Hagen-Poiseuille's Law can be used as in Eq. (2).

$$R_f = \frac{128\mu L}{\pi D^4} \tag{2}$$

Air viscosity for laminar airflow can be calculated according to Eq. (3), obtained from Gottlieb and Ritzel (1979), assuming temperature T in Kelvin, where the constant $a_o = 1.47.10^{-6} kg/(msK^{0.5})$ and Sutherland's constant is $S = 113K$.

$$\mu = \frac{a_o T^{1.5}}{T+S}\left[1 + 1.53.10^{-4}\left(\frac{T}{S} - 1\right)^2\right] \tag{3}$$

2.2 Pneumatic Capacitance (C_f)

Pneumatic capacitance represents the flow storage component as defined by Eq. (4).

$$C_f = \frac{f}{de/dt} \equiv \frac{Q}{dP/dt} \tag{4}$$

We may write $Q = dV/dt$. If we consider as positive sense the flow that goes out of a pipe, then a positive airflow ($dV/dt > 0$) causes a reduction on the pressure ($dP/dt < 0$) inside a pipe. Then we may write $C_f = (-dV/dT)/(dP/dt)$ and, simplifying this, we may write $C_f = -dV/dP$. Applying the Bulk's module definition from Eq. (5) we may write capacitance in terms of Bulk's module (Eq. (6)).

$$\beta = -V\left(\frac{dP}{dV}\right) \tag{5}$$

$$C_f = \frac{V}{\beta} \tag{6}$$

Assuming an adiabatic transformation (PV^γ remains constant), then Bulk's module becomes $\beta = \gamma P$. In order to consider the pipe length ($L = V/A$), we can then write the capacitance C_f according to Eq. (7).

$$C_f = \frac{AL}{\gamma P} \tag{7}$$

2.3 Pneumatic Inductance (I_f)

Pneumatic Inductance represents the effort storage component as defined by Eq. (8), where pressure (P) represents the pressure difference between the two ends of a pipe section.

$$I_f = \frac{e}{df/dt} \equiv \frac{P}{dQ/dt} \tag{8}$$

If we apply Newton's 2^{nd} law for the airflow considering $F = PA$ and $Q = Av$, we may write $PA = (\rho AL)\dot{Q}/A$. Rearranging this leads to Eq. (9).

$$I_f = \rho\frac{L}{A} \tag{9}$$

2.4 Inertia Forces

In order to evaluate the longitudinal acceleration effect, we propose here to consider the pipeline installed in a non-inertial reference. This will create an inertia force acting in an volume element inside the pipeline in such a way that the resulting acceleration has the same magnitude and opposite sense (Fig. 2) in comparison with the aircraft acceleration.

The pneumatic effect of inertia force is calculated as $\rho A\delta L\dot{v} = \delta PA$. This equation can be rearranged and written as Eq. (10).

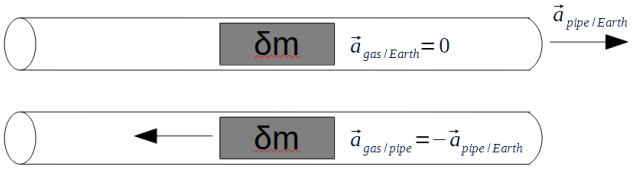

Figure 2. Inertia force acting on a mass (δm) inside a small control volume

$$P = L\rho g n_x \tag{10}$$

2.5 Bond-Graph Model

A bond-graph model is herein developed for an element of volume given by $V_i = AL_i$ inside a pipeline. Such model is composed of basic elements (**Rf**, **Cf**, **If** and **MSe**) detailed below. This modeling is performed according to theory from de Silva (2018).

Rf is a dissipative element with value given by Eq. (2); **Cf** is a flow storage element with value given by Eq. (7); **If** is an effort storage element with value given by Eq. (9). In order to represent the inertia forces, we used a **MSe**, a modulated

source of effort. Its equation can be obtained simply by using the effort-flow equivalence (in this case, using $e = P$). Thus, Eq. (10) becomes equal to Eq. (11).

$$MSe = \rho g n_x L_i \tag{11}$$

Admitting an effort e_1 as an input to the volume element, we propose a series-connected resistance R_f, followed by a parallel-connected capacitance C_f, which is then followed by a series connection of inductance I_f and the modulated source of effort MSe. The connections are modeled in Eq. (12).

$$\begin{cases} e_1 - e_2 = R_f f_1 \\ C_f \dot{e_2} = f_1 - f_2 \\ I_f \dot{f_2} + MSe = e_2 - e_3 \end{cases} \tag{12}$$

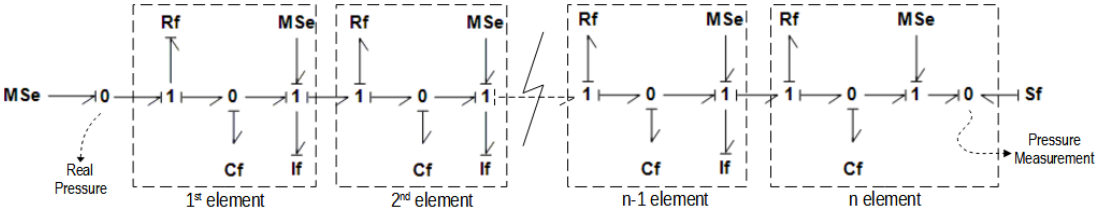

Figure 3. Pipeline complete BG model

Bond-Graphs are composed by common effort (**0**) and common flow (**1**) junctions. The graphical representation of the complete BG model is depicted on Fig. 3. Note that, to represent the blocked line end at the transducer, we added a source of flow **Sf** equal to zero.

Some signal blocks have been added surrounding the BG model blocks in order to represent the external pressures on Pitot tube. Static pressure is modeled as a function of pressure-altitude (ft) according to ISA model in ICAO (1993) in Eq. (13). Real airspeed is calculated by integrating a constant acceleration a_X (Eq. (14) and is given in terms of true airspeed (V_t). Real total pressure ($P_{t_{real}}$) is modeled as a function of V_t (Anderson (2010)), static pressure (P_s) and the speed of sound (Eq. (15)), which is a function of temperature during the test ($V_{sound} = \sqrt{\gamma R_{Air} T_{test}}$).

Measured calibrated airspeed ($V_{c_{measured}}$) is calculated based on the measured pressure according to Eq. (16) (Anderson (2010)) in the transducer line end, using the speed of sound ($V_{sound_{SL}}$) and standard atmospheric pressure ($P_{s_{SL}}$), both on sea level. The real calibrated airspeed is obtained as per Eq. (17).

The complete simulation model comprises the BG sub-models as well as auxiliary simulation blocks detailed above. A screenshot of the model implemented on 20-sim tool is depicted on Fig. 4.

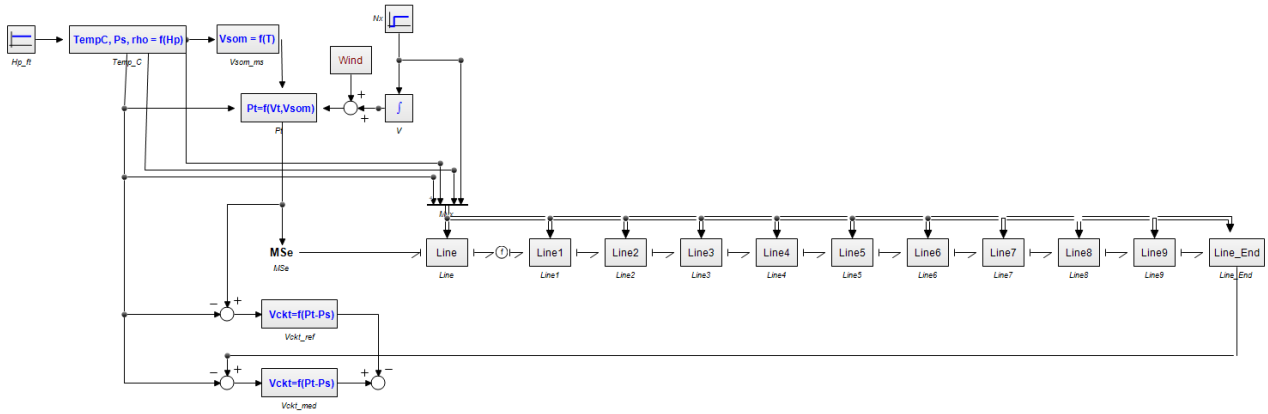

Figure 4. Simulation diagram as implemented on 20-sim

$$P_s = P_{s_{SL}} \left(1 - \frac{0.00649 H_p}{288.19}\right)^{5.256} \tag{13}$$

$$V_{t_{real}}(t) = \int_{t_0}^{t} a_X \, dt \tag{14}$$

$$P_{t_{Real}}(t) = P_s \left[0.2 \left(\frac{V_{t_{real}}(t)}{V_{sound}} \right)^2 + 1 \right]^{3.5} \tag{15}$$

$$V_{c_{measured}}(t) = V_{sound_{SL}} \sqrt{5 \left(\frac{P_{t_{measured}}(t) - P_s}{P_{s_{SL}}} + 1 \right)^{2/7} - 1} \tag{16}$$

$$V_{c_{real}}(t) = V_{sound_{SL}} \sqrt{5 \left(\frac{P_{t_{real}}(t) - P_s}{P_{s_{SL}}} + 1 \right)^{2/7} - 1} \tag{17}$$

3. SIMULATION RESULTS

Several simulations have been made using the model above described. Error plots presented on sections below indicate the measured values minus real ones. Pressure error is calculated according to Eq. (18); airspeed error is calculated according to Eq. (19). Except when mentioned, each simulation was performed assuming the parameters summarized by Tab. 3. Simulations evaluate the representation of some aspects as detailed below.

$$P_{t_{error}}(t) = P_{t_{measured}}(t) - P_{t_{real}}(t) \tag{18}$$

$$V_{c_{error}}(t) = V_{c_{measured}}(t) - V_{c_{real}}(t) \tag{19}$$

Initially, a simple acceleration simulation is presented on section 3.1. Then, the effect of inertia forces can be assessed by results presented on section 3.2. Several flight test altitudes are then evaluated on section 3.3 in order to evaluate whether or not the use of different test runways may be significant. As atmospheric temperature is a variable not controllable, its effect is also presented on section 3.4. Effects due to line specifications are also presented. Line length required by an installation is evaluated on section 3.5. Line internal diameter is also determined to present a significant effect on measured pressures, as presented on section 3.6.

A brief discussion related to simulations below is presented on section 3.7.

Table 3. Simulation Parameters

Parameter	**Value**
Pressure Altitude (ft)	2,000
Atmospheric temperature (°C)	25
Cabin temperature (°C)	22
Pipeline length (m)	22
Pipeline internal diameter (in)	1/4
Ground acceleration (g)	30%
Brakes release time (s)	10
Time frame (s)	30

Some aspects should also be considered regarding the results presented below:

- **Step-input**: Results have been obtained assuming a step-input on aircraft ground acceleration, what may not be the case in a real test;
- **Transducer chamber**: Real transducers may have an internal chamber connected to the pressure input port. Effects of such chamber on measured pressured were not considered here as the model did not consider such characteristic.
- **Longitudinal length**: Analysis presented considers a straight pipeline installed longitudinally inside aircraft cabin. Real installations, as a practical means, may present curves. As inertia forces only act in direction of acceleration, curves will add pneumatic inertia and resistance. Such effect is not considered here.
- **Pitot pressure loss**: Pneumatic resistance on Pitot tube port was not modeled. In case this resistance is comparable to pressure losses inside the pipeline some improvements on the model may be necessary.

3.1 Acceleration without inertia forces

The first simulation was made in order to evaluate the dynamics of the system and its effect on measurement errors in terms of total pressure and airspeed. Figure 5 presents the results obtained for a simulation assuming the parameters from Tab. 3 with winds calm.

Results indicate that pressure errors increase linearly with airspeed, while airspeed error, after a brief peak value of approximately -0.32kt, remain constant at -0.16kt during the rest of the time frame considered.

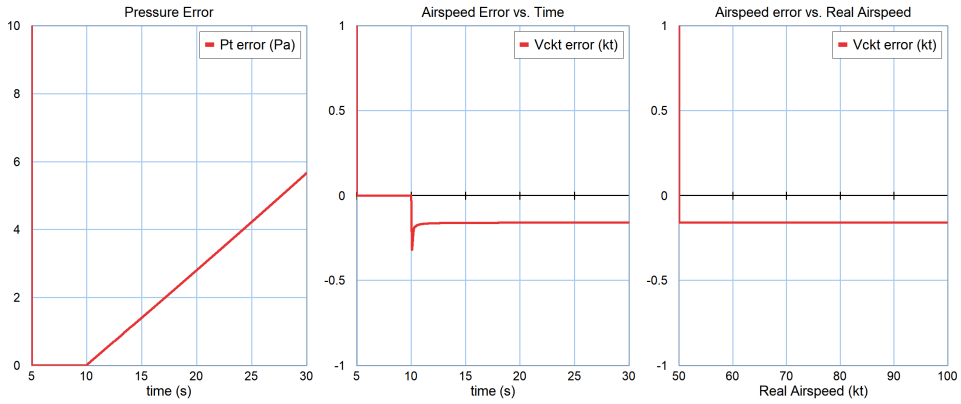

Figure 5. Simulation results without inertia forces effect

3.2 Acceleration with inertia forces

The second simulation was made in order to evaluate the dynamics of the system considering the effect of inertia forces acting on the gas inside the pipeline. Measurement error in terms of total pressure and airspeed are presented in figures below. Parameters from Tab. 3 were assumed with winds calm.

Results presented on Fig. 6 indicate the pressure at different pipeline sections, as indicated on Tab. 4. The results indicate a phenomenon similar to "water hammer", as pressure increases with the distance of the section from the total pressure probe (line input). Furthermore, there is a high frequency dynamics that vanishes after approximately 300ms.

Table 4. Simulation Parameters

Parameter	Description
Pt real	pressure at Pitot tube
P 1	pressure at 2^{nd} element (3m)
P 5	pressure at 5^{th} element (11m)
Pt end	pressure at pipeline end (22m)

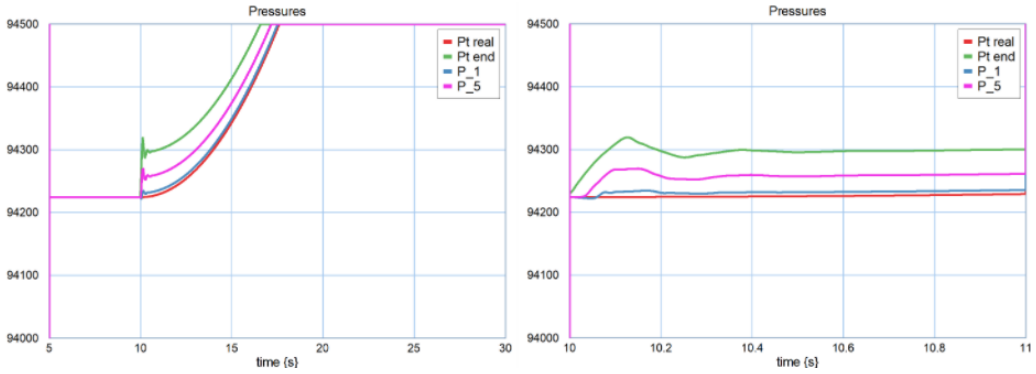

Figure 6. Simulation results pressure at different points of the pipeline

Results presented on Fig. 7 indicate that pressure errors, after a brief peak value of approximately -95Pa, remain constant at -69Pa during the rest of simulation time frame. Airspeed error also presents an initial peak value (23kt), decreasing down to 1.9kt at the end of simulation.

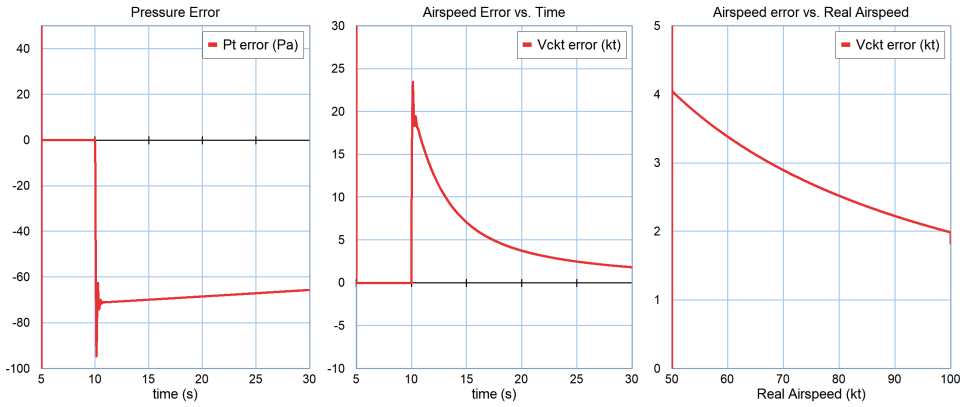

Figure 7. Simulation results with inertia forces effect

3.3 Pressure Altitude Effect

Real flight test programs may be conducted using more than one runway. Additionally, as atmospheric pressure is a variable not controlled, to assess its effect may be important for practical purposes.

Measured errors decrease in absolute value with the altitude increase. This suggests that the air density plays an important role as the smaller the air density, smaller is the pressure on the transducer end due to inertia forces. Indeed, such correlation is presented on Eq. (10). Figure 8 presents results for sea level (light red) and 5,000ft (red) conditions.

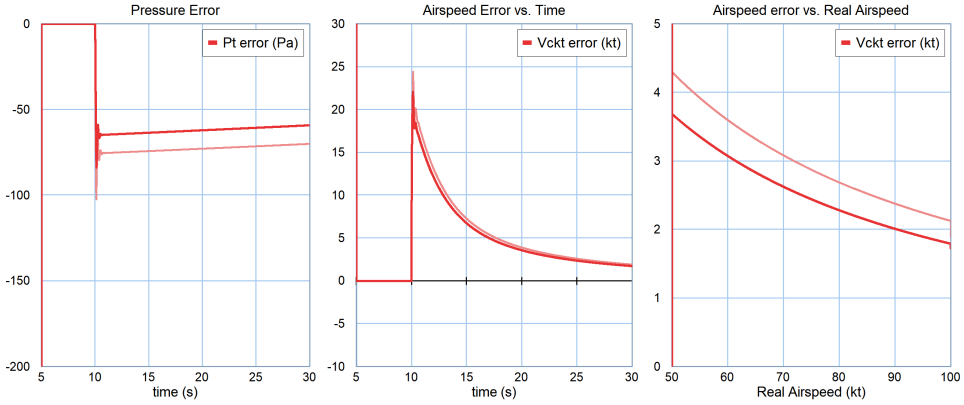

Figure 8. Simulation results for sea level (light red) and 5,000ft (red) altitudes

3.4 Atmospheric temperature Effect

Flight test programs are often extensive, requiring more than one year for a complete test program to be concluded. Thus, it is possible that some tests are performed during Winter while others occur in the Summer. As atmospheric temperature is a variable not controlled, to assess its effect may be important for practical purposes.

Measured errors decrease in absolute value with the temperature increase. This corroborates with the statement on section above that air density plays an important role as high temperatures lead to small air densities, and small pressure on the transducer end due to inertia forces. Indeed, such correlation is presented on Eq. (10). Figure 9 presents results for 0°C and 25°C conditions.

3.5 Line Length Effect

The effect on the indication errors due to the line length could be assessed by a batch simulation from an arbitrary element length minimum of 0.15m to a maximum of 0.95m with 0.2m step.

Measured errors increase with line increase as the line element length (L on Eq. (10)) is directly correlated with pressure increase due to inertia forces. Simulation results are depicted on Fig. 10.

3.6 Line Internal Diameter

The effect of line transversal area was evaluated by a simulating several internal diameters.

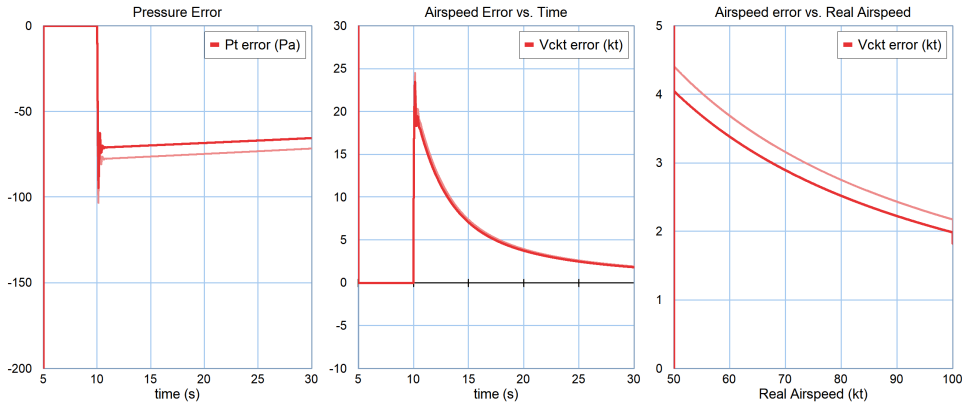

Figure 9. Simulation results for 0°C (light red) and 25°C (red)

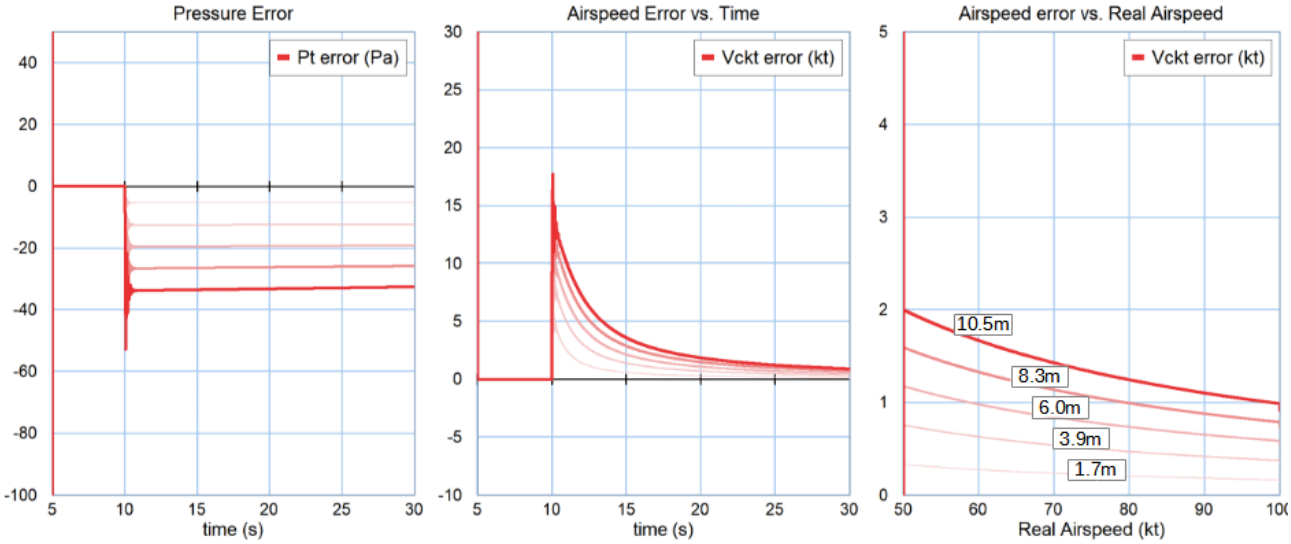

Figure 10. Simulation results for several pipeline lengths

Equation (10) presents no correlation between pressure increase due to inertia forces and line transversal area (or internal diameter). On the other hand, internal diameter directly affects pneumatic characteristics as an internal diameter reduction increases pneumatic resistance R_f (Eq. (2)), reduces pneumatic capacitance C_f (Eq. (7)) and increases pneumatic inductance I_f (Eq. (9)).

The final result due to a reduction on internal diameter is a reduction on measured airspeed errors as presented on Fig. 11. We can see that as the transversal area reduces, the measured errors decrease, even changing the signal for very thin pipelines (thinner than 0.10in).

3.7 Results Discussion

Certification rules require airspeed sensors to be calibrated on ground from 80% of the minimum V1 up to the maximum V2 (CFR 14 §25.1323(b)(1)). The airspeed lower limit may be roughly assumed equal to 60kt for jet airplanes. Certification requirements (CFR 14 §25.1323(c)) allow for a maximum error equal to 5kt at low speeds.

EASA (2007), on section 6(d)(6), states that "*the accuracy of the V1 speed should either 1) be within 1.5 knots of the V1 speed used to calculate the take-off and accelerate-stop distances, or 2) not cause an increase to these distances of more than the greater of 100 feet or the incremental increase resulting from a 1.5 knots variation in V1 speed*".

Let us consider the highest tolerable error for calibration purposes equal to 1kt. Considering the rationale described above as a region of interest, it can be seen from results presented (Fig. 10) that third line is the one that would have the higher tolerable error the 1kt at 60kt. This line corresponds to an element length equal to 0.55m. Considering that our model has 11 elements, we may conclude that pipeline lengths up to 6m would be adequate for flight test instrumentation installation.

Using the procedure described above, a maximum pipeline length can be determined for a given internal diameter. It is worth to notice that, for some internal diameters, the maximum airspeed error may be positive while, for other diameter values, it may be negative (Fig. 12). This may be explained by noticing that the there is a non-linear effect on the

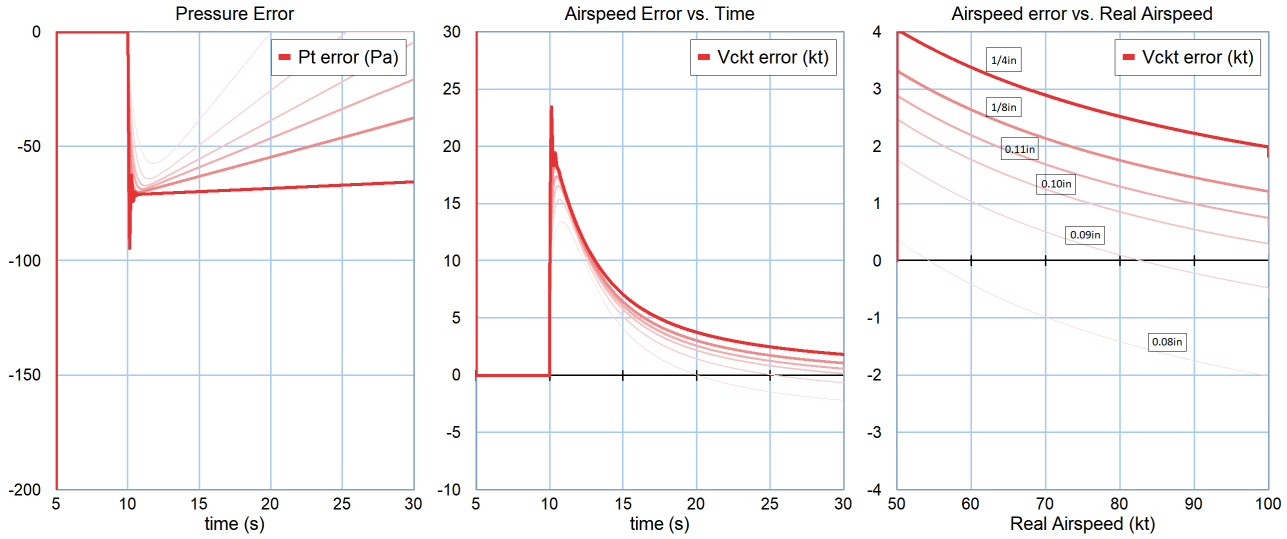

Figure 11. Simulation results for several pipeline internal diameters

pneumatic resistance (Eq. (2)) due to a reduction on internal diameter, causing, ultimately, an increase on pressure lag.

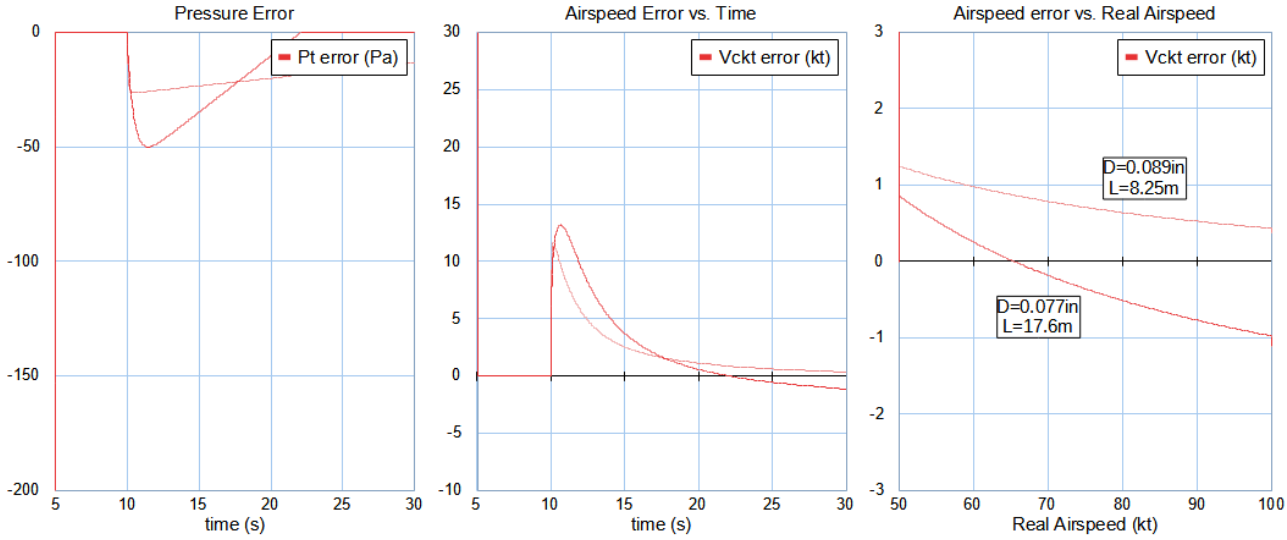

Figure 12. Error signal change for two acceptable installations (internal diameter vs. length)

Using the results obtained as above detailed, it is possible to build a chart correlating the maximum length for a determined internal diameter. Such chart is presented on Fig. 13.

4. CONCLUSIONS

A simple BG model with 11 elements of line was built. The proposed model does not use normal modes as presented by Yang *et al.* (2012) and Yang and Moan (2013). Despite its simplicity, the assumption of inertia forces effect made it possible to reproduce short-period transient responses to an acceleration step-input signal, resembling a water-hammer effect.

Sensitivities due to simulation parameters such as altitude, temperature, line length and internal diameter could be assessed. In practical terms, as line length and diameters depends on installation project, these represent the controllable variables. Results show that line length and internal diameter could be adjusted for error optimization. As longer lines may present higher errors, thinner lines could reduce those at least in a specific speed range.

A rationale based on certification requirements and guidelines was presented on section 3.7. Based on that, a guideline for the maximum tolerable length for pneumatic Pitot tubes installations could then be determined (Fig. 13).

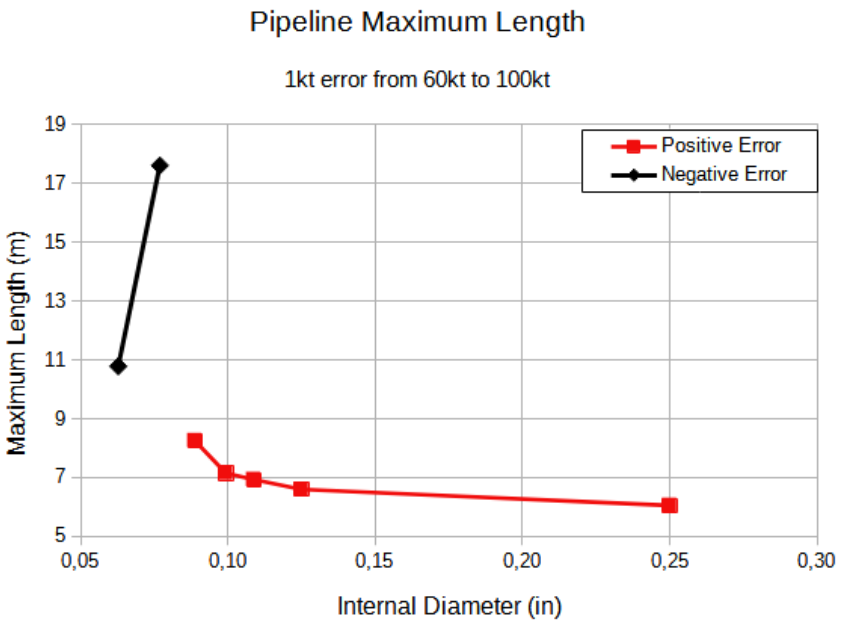

Figure 13. 1kt error chart for length vs. internal diameter

5. ACKNOWLEDGEMENTS

The authors would like to thank EMBRAER S.A. and Instituto Tecnológico de Aeronáutica (ITA) for the support during the development of this work.

6. REFERENCES

Anderson, J., 2010. *Fundamentals of Aerodynamics*. McGraw-Hill Education. ISBN 9780073398105.

de Silva, C.W., 2018. *Dynamic Systems with Engineering Applications*. CRC Press, Boca Raton, FL.

EASA, 2007. "Cs-25 book2 - acceptable means of compliance". Certification Specifications for Large Aeroplanes CS-25.

FAA, 2018. "Ac 25-7d - flight test guide for certification of transport category airplanes". Federal Aviation Administration (FAA) Advisory Circular.

Gottlieb, J.J. and Ritzel, D.V., 1979. "A semi-empirical equation for the viscosity of air". Suffield Technical Note No. 454 July, 30 1979.

Grava, A.M., Grava, C. and Novac, M., 2015. "Bond-graph modeling of the equivalent rl and rc scheme of the circuits composing an electrical transmission line". In *2015 13th International Conference on Engineering of Modern Electric Systems (EMES)*. pp. 1–4. doi:10.1109/EMES.2015.7158413.

ICAO, 1993. *Manual of the ICAO Standard Atmosphere: Extended to 80 Kilometres (262 500 Feet)*. Doc (International Civil Aviation Organization 7488-CD. International Civil Aviation Organization. ISBN 92-9194-004-6.

Prsic, D., Nedic, N. and Dubonjic, L., 2013. "Modeling and simulation of hydraulic long transmission line by bond graph". *Journal of Mechanics Engineering and Automation*, Vol. 3, pp. 257–262. doi:10.17265/2159-5275/2013.04.010.

Yang, L., Hals, J. and Moan, T., 2012. "Comparative study of bond graph models for hydraulic transmission lines with transient flow dynamics". *Journal of dynamic systems, measurement, and control*, Vol. 134, No. 3.

Yang, L. and Moan, T., 2013. "Bond graph representations of hydraulic pipelines using normal modes with dissipative friction". *SIMULATION*, Vol. 89, No. 2, pp. 199–212. doi:10.1177/0037549712469428. URL `https://doi.org/10.1177/0037549712469428`.

7. RESPONSIBILITY NOTICE

The authors are solely responsible for the printed material included in this paper.